Existence of solid Na–Xe compounds at the extreme conditions of Earth's interior

Min Zou,[1] Kang Yang,[1] Pan Zhang,[1,2] Wenwen Cui,[1] Jian Hao,[1] Jingming Shi,[1,*] and Yinwei Li[1,†]

[1]*Laboratory of Quantum Functional Materials Design and Application, School of Physics and Electronic Engineering, Jiangsu Normal University, Xuzhou 221116, China*

[2]*School of Sciences, Xinjiang Institute of Technology, Akesu 843100, China*

(Received 30 May 2023; revised 15 August 2023; accepted 9 October 2023; published 2 November 2023)

Previous studies have suggested that high pressure may induce chemical activity in noble gases (He and Xe), resulting in the emergence of high-pressure compounds containing these elements. By using first-principles theory and crystal structural prediction methods, we propose that six unconventional stoichiometries, namely, Na_2Xe, NaXe, Na_2Xe_3, $NaXe_2$, $NaXe_3$, and $NaXe_4$, can be stabilized at pressures ranging from 48 to 400 GPa, which is the highest pressure considered in this study. All the predicted Xe-containing compounds exhibit metallic properties with strong ionic Na–Xe bonds. Further *ab initio* molecular dynamics simulations show that NaXe, $NaXe_3$, and $NaXe_4$ remain in the solid state under extreme conditions, such as those present in the Earth's mantle, at pressures up to 135 GPa and temperatures up to 5000 K. This suggests that Na–Xe compounds might be possible constituents inside the Earth's mantle. These findings not only enhance our understanding of the Earth's interior, but also provide insights into Xe chemistry.

DOI: 10.1103/PhysRevResearch.5.043107

I. INTRODUCTION

Pressure is one of the most effective factors to design novel materials [1–3]. In recent years, many functional materials have been predicted to form under high-pressure conditions, but they can be synthesized and applied at ambient conditions. [4–6]. This strategy works mainly because pressure can redistribute the valence electrons and bonding pattern and reorder the energies of out atomic orbitals, which induce the new chemical valence states of elements at high pressure, and thus provide the possibility of emergence for the novel materials. These high-pressure materials always exhibit extraordinary properties, making them potential functional materials, such as superconductors [7–15] and photovoltaic materials [16,17]. Furthermore, the interiors of planets, which serve as a natural environment of high pressure and high temperature (HPHT), offer a fertile ground for the development of innovative materials. For example, Mao *et al.* found the novel maohokite, which is one of the main kinds of minerals that can exist in the interior of the Earth [18]. Therefore, research on condensed matter under high pressure has become an increasingly important topic, with implications not only for materials science but also for geoscience.

Recently, combining density function theory and structural prediction methods, scientists have made significant strides in material design and planetary understanding. In 2018, Li *et al.* proposed an effective route through He incorporation to design the high-energy density material from polymerized nitrogen under high pressure [19]. *Ab initio* molecular dynamical (AIMD) simulations and machine learning molecular dynamical simulations have provided strong evidence that superionic or liquid H_2O [20–25], NH_3 [26–28], NH_3–H_2O [29,30], NH_3–He [31,32], CH_4–He [33], and H_2O–He [5,34] could exist inside icy planets, and some of these findings (such as H_2O, NH_3, and NH_3–H_2O) are consistent with experimental results [35–38]. These findings have provided significant implications for our comprehension of planetary interiors. Typically, the noble gas Xe exhibits no chemical reactivity under ambient conditions, and previous research predicted that the interior of the Earth might be viewed as a big Xe reservoir. Therefore, the search for novel Xe-containing compounds under high pressure has become a hot topic in the planetary science and high-pressure physics. Owing to advancements in computational power and structural prediction methods, numerous Xe-containing compounds have been predicted or synthesized under extreme conditions, such as Xe–Fe/Ni [39–41], Xe–FeO_2 [42], Xe–Mg [43], Xe–N [44], Xe–Cl [45,46], Xe–O [47–51], Xe–F [52], Xe–H_2O [53], and NH_3–Xe [54]. These unconventional compounds might act as potential constituents that exist inside the inner of the Earth and provide essential information to understand the "missing Xe paradox." Although recent studies have shown that stable compounds can be formed from xenon and alkali metals (Li [55], Cs [56], Na [57], K [57], Rb [57]) under high pressure, extensive investigation into the structure and stable stoichiometries of Xe and Na under high pressure remains crucial to understand the structural models of Earth's interior, given the complex environment, diverse element ratios, and sixth abundant element of Na inside the Earth interior.

*jingmingshi@jsnu.edu.cn
†yinwei_li@jsnu.edu.cn

In this study, we conducted a systematic structure search on the Na–Xe system under high pressure. Our calculations reveal that six chemical stoichiometries, namely, Na_2Xe, NaXe, Na_2Xe_3, $NaXe_2$, $NaXe_3$, and $NaXe_4$, have negative formation enthalpies and locate on the convex hull at high pressure, indicating their stability and potential for experimental synthesis. Compared with previous study [57], we propose three unconventional chemical stoichiometries of Na_2Xe, Na_2Xe_3, and $NaXe_2$ to be stable under higher pressures. All the predicted Xe-containing compounds exhibit metallic properties with strong ionic Na–Xe bonds. Further AIMD simulations have revealed that these three compounds exhibit solid characteristics at high temperatures, corresponding to the extreme conditions of the Earth's mantle layer, suggesting that they might be possible constituents inside the Earth. These findings provide crucial insights into Xe chemistry as well as the interior models of the Earth.

II. COMPUTATIONAL DETAILS

The structure predictions for the Na–Xe system were performed by using the particle swarm optimization algorithm as implemented in the CALYPSO code [58–61]. CALYPSO is based on a global minimization of free-energy surfaces, designed for searching for a stable structure that is unbiased by any known structural information, and has successfully been used on various known systems, ranging from elements [62] to binary [63–65] and ternary [10,66] compounds. The total energy of the structure was calculated in the framework of density functional theory as implemented in the VASP code [67,68], adopting the Perdew-Burke-Ernzerhof [69] parametrization under generalized gradient approximation [70,71]. All-electron projector augmented wave pseudopotentials with $2p^6 3s^1$ and $5s^2 5p^6$ valence electrons were chosen for the Na and Xe atoms, respectively. We employed a plane-wave cutoff energy of 1000 eV and a dense Monkhorst-Pack Brillouin zone integration grid with a resolution of $2\pi \times 0.02\,\text{Å}^{-1}$. The phonon calculations were performed for all structures by using a supercell method as implemented in the PHONOPY code [72]. AIMD was performed in the canonical ensemble applying the Nosé-Hoover thermostat [73] combined with a supercell method (250 atoms for NaXe, 256 atoms for $NaXe_3$, and 240 atoms for $NaXe_4$) with the Γ point for the Brillouin zone sampling to determine the dynamical properties at high temperatures. Each simulation consists of 10 000 time steps with a time step of 1 fs. The crystal structures and electron localization function (ELF) were plotted using the VESTA software [74].

III. RESULTS AND DISCUSSION

We extensively predicted the structural stability of Na–Xe systems (Xe ∼ 1–4, Na ∼ 1–4) at pressures of 50, 100, 200, 300, and 400 GPa with maximum atoms in searching for a cell up to 40 atoms for each selected composition. We selected at least 10 lowest potential structures from all of the valid structures, which is more than 2000 for each strategy. After performing accurate optimization for the selected candidates, we calculated the formation enthalpies for each stoichiometry based on the decomposition of solid Na and Xe. Our calculations employed various phases of Xe, including the $Fm\bar{3}m$ and $P6_3/mmc$ phases [75], and multiple phases of Na, including the $Im\bar{3}m$, $Fm\bar{3}m$, $I\bar{4}3d$, $Pnma$, $tI19$, and $P6_3/mmc$ phases [76], at pressures ranging from 0 to 400 GPa. The formation enthalpy is defined as $\Delta H = [H(Na_xXe_y) - xH(Na) - yH(Xe)]/(x + y)$ and depicted in the convex hull, as shown in Fig. 1(a). At 50 GPa, a particular NaXe stoichiometry exhibits a negative formation enthalpy and is found on the convex hull, indicating energetic stability at this pressure. As pressure increases to 100 and 200 GPa, in addition to NaXe, two unconventional stoichiometries, $NaXe_3$ and $NaXe_4$, appear on the convex hull. When the pressure is raised to 300 GPa, $NaXe_4$ becomes unstable and $NaXe_2$ and a Na-rich compound Na_2Xe become energetically favorable, while the stability of Na_2Xe_3 requires an even higher pressure of 400 GPa. In addition, at compositions very close to the convex hull, such as Na_3Xe_2 at 400 GPa, we calculated its enthalpy difference relative to NaXe and Na_2Xe, which is approximately 5 meV/atom, indicating that Na_3Xe_2 might be a possible metastable phase of the Na–Xe system at this condition.

To determine the stable pressure ranges for the six predicted compositions of the Na–Xe system, we calculated their formation enthalpies with respect to all stable decompositions as a function of pressure. The phase diagram is determined and depicted in Fig. 1(b). At pressure below 100 GPa, there are three compositions, i.e., NaXe, $NaXe_3$, and $NaXe_4$, that are energetically stable, which is consistent with previous theoretical work [57]. The NaXe compound becomes stable at about 48 GPa with a large range of stable regions and remains stable up to 400 GPa, the maximum pressure that we considered. The NaXe exhibits a well-known CsCl-type structural configuration with a symmetry of $Pm\bar{3}m$. Both Xe and Na are eight coordinated in this phase and the distance between them is about 2.82 Å at 50 GPa, as shown in Fig. 2(a). $NaXe_3$ is stable in the pressure range from 71 GPa and up to 400 GPa, and with the symmetry of $Cmcm$. This structure can be viewed as a $CaIrO_3$-type ("post-perovskite") structure with each Na atom coordinated by eight Xe atoms, which can be obtained by removing the small cation Ir and replacing Ca with Na, and O with Xe, as shown in Fig. 2(b). $NaXe_4$ has a monoclinic $C2/m$ structure and is stable in the range of 87 to 261 GPa. This structure has a layered configuration, with the Xe and Na atoms arranged approximately in straight lines along the a and c axes, respectively [Fig. 2(c)].

At higher pressures, three unconventional stoichiometries, i.e., Na_2Xe, $NaXe_2$, and Na_2Xe_3, are predicted to be stable. The compound Na_2Xe, which is rich in sodium, becomes stable at 224 GPa and exhibits $Imma$ symmetry. Its configuration consists of two similar layers, as illustrated in Fig. 2(d). The two layers have comparable configurations, resembling zigzag chains of Xe atoms, while the Na atoms are arranged roughly in a straight line. $NaXe_2$ becomes stable at about 298 GPa with $I4/m$ symmetry [Fig. 2(e)]. The $NaXe_2$ has a very interesting configuration, which consists of alternating Xe and Na layers with the Xe–Xe distance of 2.64 Å and Xe–Na distance of 2.36 Å at 300 GPa. When pressure increases to 337 GPa, Na_2Xe_3 becomes stable and retains its stability up to 400 GPa. The Na_2Xe_3 has $P4/mbm$ symmetry and consists of two layers. One layer comprises four Xe atoms, while the

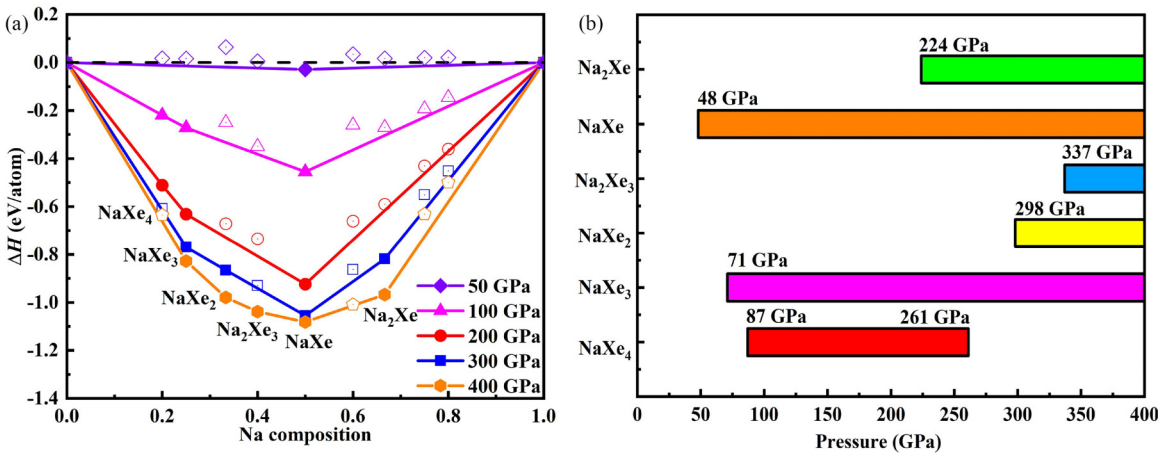

FIG. 1. Phase stabilities of Na–Xe compounds. (a) Calculated enthalpies of Na–Xe compounds with respect to the decomposition of Xe and Na at high pressures. Solid triangles, diamonds, hexagons, circles, and squares represent the stable structures. (b) Stable pressure ranges for Na_2Xe, NaXe, Na_2Xe_3, $NaXe_2$, $NaXe_3$, and $NaXe_4$ compounds.

other one contains five Xe atoms and four Na atoms, with five Xe atoms located in the vertexes and center of the lattice and four Na atoms filling in the interspace between the Xe atoms [Fig. 2(f)]. The Xe–Xe, Na–Xe, and Na–Na distances are about 2.66 Å, 2.32 Å, and 3.09 Å at 340 GPa, respectively. We also calculated the nearest Na–Xe distances of all the predicted Na–Xe compounds as a function of pressure, as shown in Fig. S1 in the Supplemental Material (SM) [77]. We observe a noticeable decrease in the distance between Na and Xe as the pressure increases, indicating a strengthening interaction between Na and Xe. For instance, in the NaXe compound, the Na–Xe bond length is approximately 2.82 Å at 50 GPa and around 2.35 Å at 400 GPa.

The absence of negative phonon dispersions of all the predicted compounds (Fig. S2 in the SM [77]) ensured their dynamical stabilities, and the electronic band structures and density of states (DOS) (Fig. S3 in the SM [77]) indicate that they all exhibit metallic properties. The DOS show that the Fermi levels are mainly occupied by the electrons from Na atoms for the $Pm\bar{3}m$-NaXe and $Imma$–Na_2Xe, while the almost equal contribution for Na and Xe atoms is obtained for the other four compounds, as shown in Fig. S3 in the SM [77]. To clarify the bond character between the Xe and Na atoms, we perform Bader charge transfer calculations and find that ∼0.58–0.72 electrons transfer from Na atom to Xe atoms, which indicates that strong ionic bonds are formed between

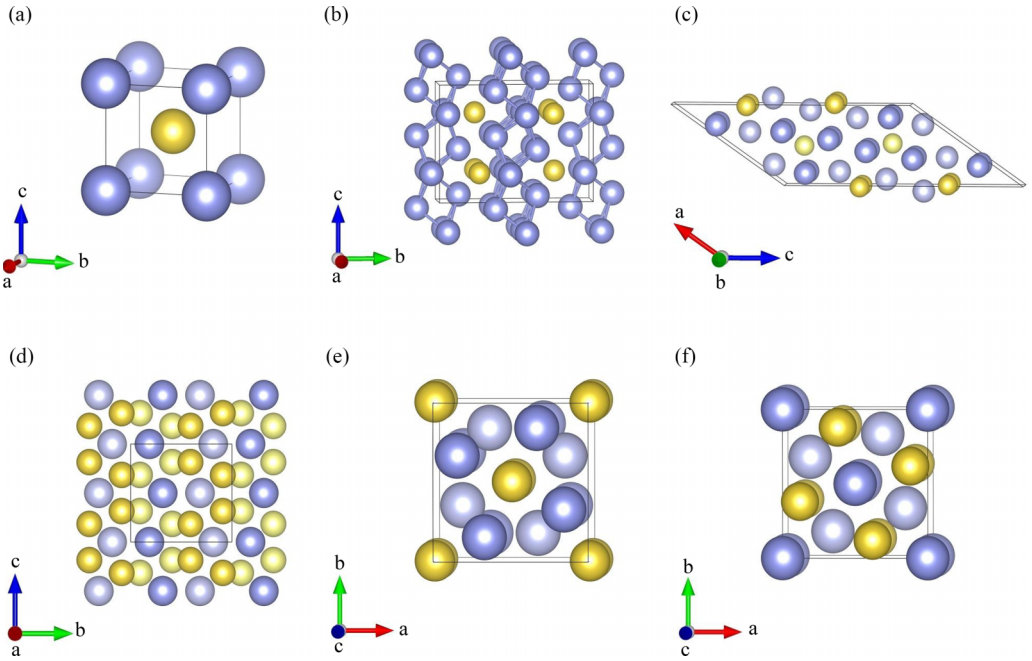

FIG. 2. Crystal structure of (a) NaXe with space group $Pm\bar{3}m$ at 50 GPa, (b) $Cmcm$ phase of $NaXe_3$ at 80 GPa, (c) $C2/m$ structure of $NaXe_4$ at 90 GPa, (d) $Imma$ phase of Na_2Xe at 230 GPa, (e) $I4/m$ structure of $NaXe_2$ at 300 GPa, and (f) $P4/mbm$ phase of Na_2Xe_3 at 340 GPa. The blue and yellow spheres represent the Xe and Na atoms, respectively.

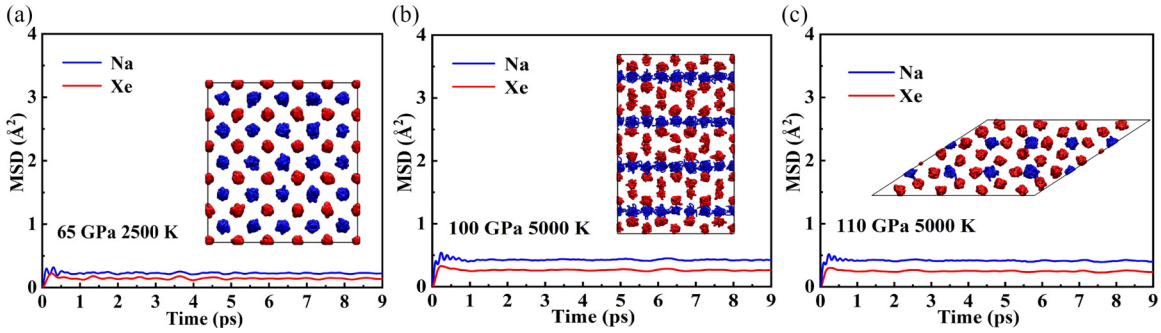

FIG. 3. The calculated mean-squared displacement (MSD) and atomic trajectories (inset) for (a) $Pm\bar{3}m$–NaXe phase at 65 GPa and 2500 K, (b) $Cmcm$–$NaXe_3$ phase at 100 GPa and 5000 K, and (c) $C2/m$–$NaXe_4$ phase at 110 GPa and 5000 K.

the Xe and Na atoms in these six predicted compounds (Table S1 and Fig. S4 in the SM [77]). This can be also confirmed by the DOS of predicted compounds with strong coupling of Na–Xe near the Fermi level. Actually, previous study shows that the He atom in Na_2He can obtain about 0.15 electrons [78], which is much smaller than that (about 1.17 electrons) in our predicted Na_2Xe. This is reasonable, as the chemical properties of Xe are more reactive than those of He, and it is easier to obtain electrons. We also calculated the Bader charge transformation between the Na and Xe atoms in the predicted compounds as a function of pressure, as shown in Fig. S4 in the SM [77] . As pressure increases, there is a slight reduction in the number of electrons lost by each Na atom in the Na–Xe compounds. The structural parameters of all the structures are summarized in Table S2 in the SM [77] .

The stable pressure ranges of the predicted Na–Xe compounds, i.e., NaXe (∼48–400 GPa), $NaXe_3$ (∼71–400 GPa), and $NaXe_4$ (∼87–261 GPa), match the extreme pressure conditions (∼0–135 GPa) of the upper mantle of the Earth. Therefore, we performed a series of AIMD calculations for these compounds at 50–135 GPa and 300–5000 K to examine their atomic dynamically properties. The calculated mean-squared displacement (MSD) and atomic trajectories of the $Pm\bar{3}m$–NaXe, $Cmcm$–$NaXe_3$, and $C2/m$–$NaXe_4$ at different pressures and temperatures are depicted in Fig. 3, and Figs. S5–S7 in the SM [77]. It is obvious that all the atoms in the $Pm\bar{3}m$–NaXe vibrate at their equilibrium positions with diffusion coefficients of zero at 65 GPa and 2500 K, which corresponds to the geotherm of the Earth, as shown in Fig. 3(a). This reveals that the $Pm\bar{3}m$–NaXe phase exhibits a solid state at this condition. As temperature increases, the $Pm\bar{3}m$–NaXe phase retains its solid character with all atoms not diffusive even at 5000 K (Fig. S5 in the SM [77]). This is mainly caused by the strong ionic Na–Xe bond, making the Na–Xe configuration difficult to destroy. This phenomenon is also observed in the $Cmcm$–$NaXe_3$ and $C2/m$–$NaXe_4$ compounds at high temperatures, as shown in Figs. 3(b) and 3(c), and in Figs. S6 and S7 in the SM [77]. We also calculated the radial distribution functions (RDFs) of Na-Xe in NaXe, $NaXe_3$, and $NaXe_4$ at different pressures and temperatures to show their solid character, as shown in Fig. S8 in the SM [77] . The RDFs reveal that at temperatures of 2000 and 5000 K, the amplitude of the Na–Xe RDFs occurs nearly at the same positions. The only difference lies in the slightly broader peak width at higher temperatures due to enhanced atomic vibrations near the equilibrium positions. Therefore, the $Pm\bar{3}m$–NaXe, $Cmcm$–$NaXe_3$, and $C2/m$–$NaXe_4$ always maintain solid characteristics in the stable pressure ranges and high-temperature conditions up to 5000 K.

We also examine the phase diagram of the $Pm\bar{3}m$–NaXe, $Cmcm$–$NaXe_3$, and $C2/m$–$NaXe_4$ at high pressures and high temperatures by comparing their Gibbs free energies (using quasiharmonic approximation to account for the temperature effects on the compounds) with individual Na and Xe, as well as all other Na–Xe compounds at different pressures and temperatures, as shown in Fig. 4. The white lines in the phase diagram represent the critical boundaries of the predicted compounds in the Na–Xe system, while the blue line represents the geotherm of the Earth. It is obvious that $Pm\bar{3}m$–NaXe, $Cmcm$–$NaXe_3$, and $C2/m$–$NaXe_4$ are stable near the Earth's geotherm and exhibit solid character (red solid points in Fig. 4) based on the AIMD simulations, which reveal that the solid Na–Xe compounds might be possible constituents at the Earth's mantle. Therefore, the predictions of the Na–Xe system could not only update the models of the Earth's interiors, but also provide strong evidence that Xe might be present in the Earth interior in the form of compounds. Moreover, Si, Mg, and Ca elements are also abundant in the inner Earth; therefore, there is a high possibility that Xe could react

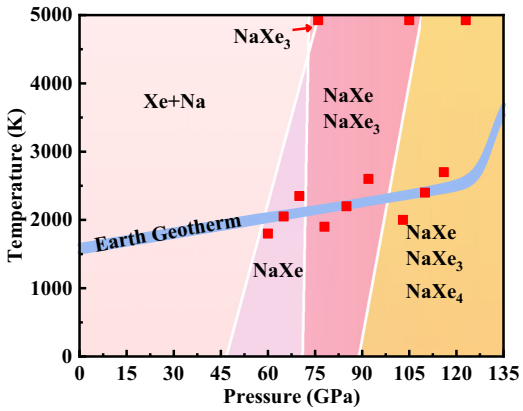

FIG. 4. Phase diagram of NaXe, $NaXe_3$, and $NaXe_4$ at high pressures and high temperatures, which corresponds to the extreme conditions of the inner Earth. The red squares represent the solid character and the white solid lines represent the phase boundaries of different compounds.

with them at high pressures to form new compounds, which deserves further investigation.

IV. CONCLUSIONS

In conclusion, we have performed extensive simulations on the structural prediction and phase stabilities of the Na–Xe system at high pressure, and proposed six unconventional stoichiometries, i.e., Na_2Xe, NaXe, Na_2Xe_3, $NaXe_2$, $NaXe_3$, and $NaXe_4$, that could stabilize in a large pressure range from 48 to 400 GPa. All the predicted Xe-containing compounds exhibit metallic properties with strong ionic Na–Xe bonds. Further *ab initio* molecular dynamics calculations show that the predicted $Pm\bar{3}m$–NaXe, $Cmcm$–$NaXe_3$, and $C2/m$–$NaXe_4$ compounds remain in the solid state at the extreme condition with the pressure up to 135 GPa and temperature up to 5000 K, corresponding to the extreme conditions of Earth's interior, which indicates that the Na–Xe compounds might be possible constituents in the mantle of the Earth. These results could not only provide essential information for understanding the interior of the Earth, but also provide strong evidence that Xe might be present in the Earth interior in the form of compounds.

ACKNOWLEDGMENTS

The authors acknowledge funding from the NSFC under Grants No. 12074154, No. 12174160, No. 11804128, and No. 11804129. Y.L. acknowledges the funding from the Six Talent Peaks Project and 333 High-level Talents Project of Jiangsu Province. All the calculations were performed at the High Performance Computing Center of the School of Physics and Electronic Engineering of Jiangsu Normal University.

M.Z. and K.Y. contributed equally to this work.

[1] L. Zhang, Y. Wang, J. Lv, and Y. Ma, Materials discovery at high pressures, Nat. Rev. Mater. **2**, 17005 (2017).

[2] M.-s. Miao, Caesium in high oxidation states and as a *p*-block element, Nat. Chem. **5**, 846 (2013).

[3] M. Xu, Y. Li, and Y. Ma, Materials by design at high pressures, Chem. Sci. **13**, 329 (2022).

[4] Q. Li, Y. Ma, A. R. Oganov, H. Wang, H. Wang, Y. Xu, T. Cui, H.-K. Mao, and G. Zou, Superhard monoclinic polymorph of carbon, Phys. Rev. Lett. **102**, 175506 (2009).

[5] C. Liu, H. Gao, Y. Wang, R. J. Needs, C. J. Pickard, J. Sun, H.-T. Wang, and D. Xing, Multiple superionic states in helium–water compounds, Nat. Phys. **15**, 1065 (2019).

[6] K. Xia, Q. Chen, H. Gao, X. Feng, J. Yuan, C. Liu, S. A. T. Redfern, and J. Sun, Icosahedral silicon boride: A potential hybrid photovoltaic-thermoelectric for energy harvesting, Phys. Rev. Mater. **5**, 115402 (2021).

[7] Y. Li, J. Hao, H. Liu, Y. Li, and Y. Ma, The metallization and superconductivity of dense hydrogen sulfide, J. Chem. Phys. **140**, 174712 (2014).

[8] D. Duan, Y. Liu, F. Tian, D. Li, X. Huang, Z. Zhao, H. Yu, B. Liu, W. Tian, and T. Cui, Pressure-induced metallization of dense $(H_2S)_2H_2$ with high-T_c superconductivity, Sci. Rep. **4**, 6968 (2014).

[9] M. Somayazulu, M. Ahart, A. K. Mishra, Z. M. Geballe, M. Baldini, Y. Meng, V. V. Struzhkin, and R. J. Hemley, Evidence for superconductivity above 260 K in lanthanum superhydride at megabar pressures, Phys. Rev. Lett. **122**, 027001 (2019).

[10] W. Cui, T. Bi, J. Shi, Y. Li, H. Liu, E. Zurek, and R. J. Hemley, Route to high-T_c superconductivity via CH_4-intercalated H_3S hydride perovskites, Phys. Rev. B **101**, 134504 (2020).

[11] Y. Sun, Y. Tian, B. Jiang, X. Li, H. Li, T. Iitaka, X. Zhong, and Y. Xie, Computational discovery of a dynamically stable cubic SH_3-like high-temperature superconductor at 100 GPa via CH_4 intercalation, Phys. Rev. B **101**, 174102 (2020).

[12] E. Snider, N. Dasenbrock-Gammon, R. McBride, M. Debessai, H. Vindana, K. Vencatasamy, K. V. Lawler, A. Salamat, and R. P. Dias, Room-temperature superconductivity in a carbonaceous sulfur hydride, Nature (London) **586**, 373 (2020).

[13] A. P. Drozdov, M. I. Eremets, I. A. Troyan, V. Ksenofontov, and S. I. Shylin, Conventional superconductivity at 203 kelvin at high pressures in the sulfur hydride system, Nature (London) **525**, 73 (2015).

[14] H. Liu, I. I. Naumov, R. Hoffmann, N. W. Ashcroft, and R. J. Hemley, Potential high-T_c superconducting lanthanum and yttrium hydrides at high pressure, Proc. Natl. Acad. Sci. USA **114**, 6990 (2017).

[15] A. P. Drozdov, P. P. Kong, V. S. Minkov, S. P. Besedin, M. A. Kuzovnikov, S. Mozaffari, L. Balicas, F. F. Balakirev, D. E. Graf, V. B. Prakapenka, E. Greenberg, D. A. Knyazev, M. Tkacz, and M. I. Eremets, Superconductivity at 250 K in lanthanum hydride under high pressures, Nature (London) **569**, 528 (2019).

[16] S. Ding, J. Shi, J. Xie, W. Cui, P. Zhang, K. Yang, J. Hao, L. Zhang, and Y. Li, Helium incorporation induced direct-gap silicides, npj Comput. Mater. **7**, 89 (2021).

[17] C. Liu, J. Wang, X. Deng, X. Wang, C. J. Pickard, R. Helled, Z. Wu, H.-T. Wang, D. Xing, and J. Sun, Partially diffusive helium-silica compound under high pressure, Chin. Phys. Lett. **39**, 076101 (2022).

[18] H.-K. Mao, T. Takahashi, W. A. Bassett, G. L. Kinsland, and L. Merrill, Isothermal compression of magnetite to 320 KB, J. Geophys. Res. **79**, 1165 (1974).

[19] Y. Li, X. Feng, H. Liu, J. Hao, S. Redfern, W. Lei, D. Liu, and Y. Ma, Route to high-energy density polymeric nitrogen *t*-N via HeN compounds, Nat. Commun. **9**, 722 (2018).

[20] V. B. Prakapenka, N. Holtgrewe, S. S. Lobanov, and A. F. Goncharov, Structure and properties of two superionic ice phases, Nat. Phys. **17**, 1233 (2021).

[21] M. Ji, K. Umemoto, C.-Z. Wang, K.-M. Ho, and R. M. Wentzcovitch, Ultrahigh-pressure phases of H_2O ice predicted using an adaptive genetic algorithm, Phys. Rev. B **84**, 220105(R) (2011).

[22] M. Benoit, M. Bernasconi, P. Focher, and M. Parrinello, New high-pressure phase of ice, Phys. Rev. Lett. **76**, 2934 (1996).

[23] M. French, T. R. Mattsson, N. Nettelmann, and R. Redmer, Equation of state and phase diagram of water at ultrahigh pressures as in planetary interiors, Phys. Rev. B **79**, 054107 (2009).

[24] B. Cheng, M. Bethkenhagen, C. J. Pickard, and S. Hamel, Phase behaviours of superionic water at planetary conditions, Nat. Phys. **17**, 1228 (2021).

[25] A. Reinhardt, M. Bethkenhagen, F. Coppari, M. Millot, S. Hamel, and B. Cheng, Thermodynamics of high-pressure ice phases explored with atomistic simulations, Nat. Commun. **13**, 4707 (2022).

[26] G. I. G. Griffiths, R. J. Needs, and C. J. Pickard, High-pressure ionic and molecular phases of ammonia within density functional theory, Phys. Rev. B **86**, 144102 (2012).

[27] J.-A. Hernandez, M. Bethkenhagen, S. Ninet, M. French, A. Benuzzi-Mounaix, F. Datchi, M. Guarguaglini, F. Lefevre, F. Occelli, R. Redmer, T. Vinci, and A. Ravasioothers, Melting curve of superionic ammonia at planetary interior conditions, Nat. Phys. **19**, 1280 (2023).

[28] M. Bethkenhagen, M. French, and R. Redmer, Equation of state and phase diagram of ammonia at high pressures from *ab initio* simulations, J. Chem. Phys. **138**, 234504 (2013).

[29] V. N. Robinson and A. Hermann, Plastic and superionic phases in ammonia–water mixtures at high pressures and temperatures, J. Phys.: Condens. Matter **32**, 184004 (2020).

[30] M. Bethkenhagen, D. Cebulla, R. Redmer, and S. Hamel, Superionic phases of the 1:1 water–ammonia mixture, J. Phys. Chem. A **119**, 10582 (2015).

[31] J. Shi, W. Cui, J. Hao, M. Xu, X. Wang, and Y. Li, Formation of ammonia–helium compounds at high pressure, Nat. Commun. **11**, 3164 (2020).

[32] C. Liu, H. Gao, A. Hermann, Y. Wang, M. Miao, C. J. Pickard, R. J. Needs, H.-T. Wang, D. Xing, and J. Sun, Plastic and superionic helium ammonia compounds under high pressure and high temperature, Phys. Rev. X **10**, 021007 (2020).

[33] H. Gao, C. Liu, A. Hermann, R. J. Needs, C. J. Pickard, H.-T. Wang, D. Xing, and J. Sun, Coexistence of plastic and partially diffusive phases in a helium-methane compound, Natl. Sci. Rev. **7**, 1540 (2020).

[34] H. Liu, Y. Yao, and D. D. Klug, Stable structures of He and H_2O at high pressure, Phys. Rev. B **91**, 014102 (2015).

[35] M. Millot, S. Hamel, J. R. Rygg, P. M. Celliers, G. W. Collins, F. Coppari, D. E. Fratanduono, R. Jeanloz, D. C. Swift, and J. H. Eggert, Experimental evidence for superionic water ice using shock compression, Nat. Phys. **14**, 297 (2018).

[36] C. Cavazzoni, G. L. Chiarotti, S. Scandolo, E. Tosatti, M. Bernasconi, and M. Parrinello, Superionic and metallic states of water and ammonia at giant planet conditions, Science **283**, 44 (1999).

[37] M. Millot, F. Coppari, J. R. Rygg, A. C. Barrios, S. Hamel, D. C. Swift, and J. H. Eggert, Nanosecond x-ray diffraction of shock-compressed superionic water ice, Nature (London) **569**, 251 (2019).

[38] A. Ravasio, M. Bethkenhagen, J.-A. Hernandez, A. Benuzzi-Mounaix, F. Datchi, M. French, M. Guarguaglini, F. Lefevre, S. Ninet, R. Redmer, and T. Vinci, Metallization of shock-compressed liquid ammonia, Phys. Rev. Lett. **126**, 025003 (2021).

[39] L. Zhu, H. Liu, C. J. Pickard, G. Zou, and Y. Ma, Reactions of xenon with iron and nickel are predicted in the Earth's inner core, Nat. Chem. **6**, 644 (2014).

[40] A. Dewaele, C. M. Pépin, G. Geneste, and G. Garbarino, Reaction between nickel or iron and xenon under high pressure, High Press. Res. **37**, 137 (2017).

[41] E. Stavrou, Y. Yao, A. F. Goncharov, S. S. Lobanov, J. M. Zaug, H. Liu, E. Greenberg, and V. B. Prakapenka, Synthesis of xenon and iron-nickel intermetallic compounds at Earth's core thermodynamic conditions, Phys. Rev. Lett. **120**, 096001 (2018).

[42] F. Peng, X. Song, C. Liu, Q. Li, M.-s. Miao, C. Chen, and Y. Ma, Xenon iron oxides predicted as potential Xe hosts in Earths lower mantle, Nat. Commun. **11**, 5227 (2020).

[43] M.-s. Miao, X.-L. Wang, J. Brgoch, F. Spera, M. G. Jackson, G. Kresse, and H.-Q. Lin, Anionic chemistry of noble gases: Formation of Mg–NG (NG= Xe, Kr, Ar) compounds under pressure, J. Am. Chem. Soc. **137**, 14122 (2015).

[44] F. Peng, Y. Wang, H. Wang, Y. Zhang, and Y. Ma, Stable xenon nitride at high pressures, Phys. Rev. B **92**, 094104 (2015).

[45] N. Zarifi and J. S. Tse, Structural search for high pressure CS_2 and Xe–Cl compounds, J. Phys. Soc. Jpn. **87**, 041014 (2018).

[46] N. Zarifi, H. Liu, J. S. Tse, and E. Zurek, Crystal structures and electronic properties of Xe–Cl compounds at high pressure, J. Phys. Chem. C **122**, 2941 (2018).

[47] A. Dewaele, P. Loubeyre, P. Dumas, and M. Mezouar, Oxygen impurities reduce the metallization pressure of xenon, Phys. Rev. B **86**, 014103 (2012).

[48] G. Weck, A. Dewaele, and P. Loubeyre, Oxygenble gas binary phase diagrams at 296 K and high pressures, Phys. Rev. B **82**, 014112 (2010).

[49] Q. Zhu, D. Y. Jung, A. R. Oganov, C. W. Glass, C. Gatti, and A. O. Lyakhov, Stability of xenon oxides at high pressures, Nat. Chem. **5**, 61 (2013).

[50] A. Hermann and P. Schwerdtfeger, Xenon suboxides stable under pressure, J. Phys. Chem. Lett. **5**, 4336 (2014).

[51] A. Dewaele, N. Worth, C. J. Pickard, R. J. Needs, S. Pascarelli, O. Mathon, M. Mezouar, and T. Irifune, Synthesis and stability of xenon oxides Xe_2O_5 and Xe_3O_2 under pressure, Nat. Chem. **8**, 784 (2016).

[52] F. Peng, J. Botana, Y. Wang, Y. Ma, and M.-s. Miao, Unexpected trend in stability of Xe–F compounds under pressure driven by Xe–Xe covalent bonds, J. Phys. Chem. Lett. **7**, 4562 (2016).

[53] C. Sanloup, S. A. Bonev, M. Hochlaf, and H. E. Maynard-Casely, Reactivity of xenon with ice at planetary conditions, Phys. Rev. Lett. **110**, 265501 (2013).

[54] P. Zhang, J. Shi, W. Cui, C. Liu, S. Ding, K. Yang, J. Hao, and Y. Li, Formation of NH_3–Xe compound at the extreme condition of planetary interiors, Phys. Rev. B **105**, 214109 (2022).

[55] Z. Liu, J. Botana, M.-s. Miao, and D. Yan, Unexpected Xe anions in XeLin intermetallic compounds, Europhys. Lett. **117**, 26002 (2017).

[56] S. Zhang, H. Bi, S. Wei, J. Wang, Q. Li, and Y. Ma, Crystal structures and electronic properties of cesium xenides at high pressures, J. Phys. Chem. C **119**, 24996 (2015).

[57] Y. Tian, S. T. John, G. Liu, and H. Liu, Predicted crystal structures of xenon and alkali metals under high pressures, Phys. Chem. Chem. Phys. **24**, 18119 (2022).

[58] Y. Wang, J. Lv, L. Zhu, and Y. Ma, Crystal structure prediction via particle-swarm optimization, Phys. Rev. B **82**, 094116 (2010).

[59] Y. Wang, J. Lv, L. Zhu, and Y. Ma, CALYPSO: A method for crystal structure prediction, Comput. Phys. Commun. **183**, 2063 (2012).

[60] B. Gao, P. Gao, S. Lu, J. Lv, Y. Wang, and Y. Ma, Interface structure prediction via CALYPSO method, Sci. Bull. **64**, 301 (2019).

[61] X. Shao, J. Lv, P. Liu, S. Shao, P. Gao, H. Liu, Ya. Wang, and Y. Ma, A symmetry-orientated divide-and-conquer method for crystal structure prediction, J. Chem. Phys. **156**, 014105 (2022).

[62] Y. Li, Y. Wang, C. J. Pickard, R. J. Needs, Y. Wang, and Y. Ma, Metallic icosahedron phase of sodium at terapascal pressures, Phys. Rev. Lett. **114**, 125501 (2015).

[63] K. Gao, W. Cui, J. Chen, Q. Wang, J. Hao, J. Shi, C. Liu, S. Botti, M. A. L. Marques, and Y. Li, Superconducting hydrogen tubes in hafnium hydrides at high pressure, Phys. Rev. B **104**, 214511 (2021).

[64] Q. Wang, W. Cui, K. Gao, J. Chen, T. Gu, M. Liu, J. Hao, J. Shi, and Y. Li, Pressure-stabilized superconducting electride Li_5C, Phys. Rev. B **106**, 054519 (2022).

[65] M. Xu, C. Huang, Y. Li, S. Liu, X. Zhong, P. Jena, E. Kan, and Y. Wang, Electrical control of magnetic phase transition in a type-I multiferroic double-metal trihalide monolayer, Phys. Rev. Lett. **124**, 067602 (2020).

[66] J. Shi, W. Cui, S. Botti, and M. A. L. Marques, Nitrogen-hydrogen-oxygen ternary phase diagram: New phases at high pressure from structural prediction, Phys. Rev. Mater. **2**, 023604 (2018).

[67] G. Kresse and J. Furthmüller, Efficient iterative schemes for *ab initio* total-energy calculations using a plane-wave basis set, Phys. Rev. B **54**, 11169 (1996).

[68] A. Vanderlei dos Santos, G. Padilha, and M. Monçalves, Determination of the stability and magnetic properties of FePd nitride using the generalised gradient approximation (GGA), Solid State Sci. **14**, 269 (2012).

[69] P. E. Blöchl, O. Jepsen, and O. K. Andersen, Improved tetrahedron method for Brillouin-zone integrations, Phys. Rev. B **49**, 16223 (1994).

[70] J. P. Perdew, J. A. Chevary, S. H. Vosko, K. A. Jackson, M. R. Pederson, D. J. Singh, and C. Fiolhais, Atoms, molecules, solids, and surfaces: Applications of the generalized gradient approximation for exchange and correlation, Phys. Rev. B **46**, 6671 (1992).

[71] J. P. Perdew, K. Burke, and M. Ernzerhof, Generalized gradient approximation made simple, Phys. Rev. Lett. **77**, 3865 (1996).

[72] A. Togo, F. Oba, and I. Tanaka, First-principles calculations of the ferroelastic transition between rutile-type and $CaCl_2$-type SiO_2 at high pressures, Phys. Rev. B **78**, 134106 (2008).

[73] W. G. Hoover, Canonical dynamics: Equilibrium phase-space distributions, Phys. Rev. A **31**, 1695 (1985).

[74] K. Momma and F. Izumi, *VESTA3* for three-dimensional visualization of crystal, volumetric and morphology data, J. Appl. Crystallogr. **44**, 1272 (2011).

[75] E. Kim, M. Nicol, H. Cynn, and C.-S. Yoo, Martensitic fcc-to-hcp transformations in solid xenon under pressure: A first-principles study, Phys. Rev. Lett. **96**, 035504 (2006).

[76] Y. Ma, M. Eremets, A. R. Oganov, Y. Xie, I. Trojan, S. Medvedev, A. O. Lyakhov, M. Valle, and V. Prakapenka, Transparent dense sodium, Nature (London) **458**, 182 (2009).

[77] See Supplemental Material at http://link.aps.org/supplemental/10.1103/PhysRevResearch.5.043107, which includes structural configurations and parameters, Bader charge, phonon dispersion, band structures, DOS mean-squared displacement (MSD), and atomic trajectories of the predicted Na–Xe compounds at different pressures.

[78] X. Dong, A. R. Oganov, A. F. Goncharov, E. Stavrou, S. Lobanov, G. Saleh, G.-R. Qian, Q. Zhu, C. Gatti, V. L. Deringer *et al.*, A stable compound of helium and sodium at high pressure, Nat. Chem. **9**, 440 (2017).